

# Physical properties of $R\text{Co}_2\text{Al}_8$ ( $R = \text{La}, \text{Ce}, \text{Pr}, \text{Nd}$ and $\text{Sm}$ ) single crystals: an emerging structure-type for anisotropic Kondo lattice studies

Fernando A. Garcia<sup>1,2,3</sup>, Sushma Kumari<sup>1,2</sup>, Juan Schmidt<sup>1,2</sup>, Cris Adriano<sup>2</sup>,  
Aashish Sapkota<sup>1</sup>, Paul C. Canfield<sup>1,2</sup>, Rebecca Flint<sup>1,2</sup> and Raquel A. Ribeiro<sup>1,2</sup>  
<sup>1</sup>Ames Laboratory, U.S. DOE, Ames, Iowa 50011, USA

<sup>2</sup>Department of Physics and Astronomy, Iowa State University, Ames, Iowa 50011, USA and

<sup>3</sup>Instituto de Física, Universidade de São Paulo, São Paulo-SP, 05508-090, Brazil

Systematic investigations of rare-earth ( $R$ ) based intermetallic materials is a leading strategy to reveal the underlying mechanisms governing a range of physical phenomena, such as the formation of a Kondo lattice and competing electronic and magnetic anisotropies. In this work, the magnetic, thermal and transport properties of  $R\text{Co}_2\text{Al}_8$  ( $R = \text{La}, \text{Ce}, \text{Pr}, \text{Nd}$  and  $\text{Sm}$ ) single crystals are presented.  $\text{LaCo}_2\text{Al}_8$  is characterized as a Pauli paramagnet and transport measurements, with the current along and perpendicular to the orthorhombic  $c$ -axis ( $\rho_c$  and  $\rho_{ab}$ , respectively), reveal a clear electronic anisotropy, with  $\rho_{ab} \approx (4 - 7)\rho_c$  at 300 K. We show that  $\text{CeCo}_2\text{Al}_8$  is a Kondo-lattice for which the Kondo coherence temperature  $T_K^*$ , deduced from broad maximums in  $\rho_c$  and  $\rho_{ab}$  at  $\approx 68$  and  $46$  K, respectively, is also anisotropic. This finding is related to a possible underlying anisotropy of the Kondo coupling in  $\text{CeCo}_2\text{Al}_8$ . The Pr and Nd-based materials present strong easy-axis anisotropy ( $c$ -axis) and antiferromagnetic (AFM) orders below  $T = 4.84$  K and  $T = 8.1$  K, respectively. Metamagnetic transitions from this AFM to a spin-polarized paramagnetic phase state are investigated by isothermal magnetization measurements. The Sm-based compound is also an easy-axis AFM with a transition at  $T = 21.6$  K.

## I. INTRODUCTION

The physical properties of rare-earth ( $R$ ) based intermetallic materials encompasses a broad phenomenology ranging from, among others, heavy fermion behavior, superconductivity and magnetism. Rich phase diagrams are found in the case of heavy fermion materials, reflecting the coexistence of energy scales competing for the material ground state. The formation of the heavy fermion state is due to the local hybridization between the rare-earth-derived  $4f$  and conduction electrons, and is more often realized in Ce- and Yb-based materials. This hybridization leads to the formation of a Kondo lattice, characterized by a many-body coherence temperature  $T_K^*$ , below which the localized and itinerant states are entangled in a liquid of heavy carriers [1–5].

The key to understanding heavy fermions is to disentangle the contributions from distinct degrees of freedom, lattice and electronic, which is usually accomplished by systematic investigations of the physical properties of a particular series. Indeed, for a given structural type, it is paramount to seek for examples of non-moment bearing (La-, Lu- and Y-based materials), pure local moment (Pr-, Nd-, Gd-Tm-based materials) and hybridizing (Ce- and Yb-based materials and, sometimes, Pr-, Sm- and Eu-based materials)  $R$ -based intermetallics. This need for a comprehensive set of physical properties is well exemplified by material series like  $R\text{Ni}_2\text{Ge}_2$  [6],  $R\text{Ni}_2\text{B}_2\text{C}$  [7–9],  $\text{RAgSb}_2$  [10, 11],  $\text{RPtBi}$  [12, 13] and  $\text{RM}_2\text{Zn}_{20}$  [14].

An ongoing topic of investigation in this field is the interaction between the Kondo lattice and the magnetic anisotropies. Indeed, the local hybridizations leading to the Kondo lattice are set by large energy scales that may compete with the crystalline electric field (CEF) determined anisotropy. This is well illustrated by the phe-

nomenology of the “hard-axis” ordering, where magnetic order develops along the (CEF determined) hard-axis of magnetization in Kondo materials [15–18]. Moreover, the subject motivates the seek of first-principles theoretical approaches to understanding CEF effects and the search for new anisotropic Ce-based materials [19, 20].

Recently, attention has been devoted to 1-2-8  $R$ -based materials adopting the  $\text{CaCo}_2\text{Al}_8$ -type orthorhombic crystal structure (space group  $Pbam$ ). In this structure, the rare-earth ( $R$ ) cations are organized along chains in the  $c$ -axis, with the  $R$ - $R$  distances being smaller along the  $c$ -axis than the distances observed when the structure is projected onto the  $ab$ -plane. In particular, some gallides ( $\text{RM}_2\text{Ga}_8$ , where  $M$  is a transition metal) have shown interesting physics, as magnetic quantum critical behavior observed in  $\text{NdFe}_2\text{Ga}_8$  [21, 22] and an axial Kondo lattice in  $\text{CeCo}_2\text{Ga}_8$  [23–26]. In the later case, an axial Kondo chain is evidenced by a strong anisotropy of the resistivity ( $\rho$ ), which shows a broad maximum (about 17 K, characterizing  $T_K^*$  for this material), only for measurements along the  $c$ -axis ( $\rho_c$ ). For measurements along  $a$  and  $b$ ,  $\rho$  keeps going up at low temperatures in a way that is reminiscent of the single ion Kondo effect (incoherent Kondo scattering). This phenomenology suggests that the underlying  $4f$ -conduction electrons hybridization is anisotropic in this material. The  $\text{CeCo}_2\text{Ga}_8$  magnetic properties are also anisotropic, with the  $c$ -axis identified as the easy-axis. The  $c$ -axis was also identified as the easy-axis for  $\text{PrFe}_2\text{Ga}_8$  [27] and  $\text{PrRu}_2\text{Ga}_8$  [28]. As for the vast majority of the  $R$ -based materials, the magnetic anisotropy is likely set by crystalline electric field (CEF) effects [25].

The  $\text{RM}_2\text{Ga}_8$  materials thus display anisotropic electronic and magnetic properties.  $\text{CeCo}_2\text{Ga}_8$ , in particular, showcases an example of coexisting hybridization

and CEF determined anisotropies. A good number of  $R$ -based aluminides ( $RM_2Al_8$ ) also adopt the  $CaCo_2Al_8$ -type orthorhombic structure. Early explorations of these materials focused on samples in polycrystalline form [29–31] until recently, when the growth of single crystals from an Al-rich ternary composition was reported [32, 33]. Our paper is dedicated to the physical properties of  $RCo_2Al_8$  ( $R = La, Ce, Pr, Nd$  and  $Sm$ ) single crystals.

We start showing that  $LaCo_2Al_8$  is a simple Pauli paramagnet which display a clear electronic anisotropy, that is characterized by a large anisotropy in resistivity ( $\rho$ ) measurements. Indeed, at  $T = 300$  K, we found that  $\rho_{ab}/\rho_c \approx 4 - 7$ , where  $\rho_c$  and  $\rho_{ab}$  are, respectively, the resistivity measured with the current along and perpendicular to the orthorhombic,  $c$ -axis. We then investigated  $CeCo_2Al_8$ .

Previously, the formation of a Kondo lattice in  $CeCo_2Al_8$  was deduced based upon the observation of a broad maximum in  $\rho(T)$  measurements of polycrystalline samples [29] but this was not observed in  $CeCo_2Al_8$  single crystals [32]. The status of  $CeCo_2Al_8$  as a Kondo lattice thus requires clarification. Here, we show that  $CeCo_2Al_8$  is an anisotropic Kondo lattice system, for which  $T_K^*$ , deduced from broad maximums in  $\rho_c$  and  $\rho_{ab}$  ( $T_{K,c}^*$  and  $T_{K,ab}^*$ , respectively), assume different values, with  $T_{K,c}^* \approx 68$  K and  $T_{K,ab}^* \approx 46$  K. This finding is examined in the light of the proposed Kondo chain in  $CeCo_2Ga_8$ .

We then investigate  $PrCo_2Al_8$  and  $NdCo_2Al_8$ .  $PrCo_2Al_8$  was shown to be a strong easy-axis antiferromagnetic (AFM) material [28]. Our experiments confirm this property of the Pr-based material and adds that  $NdCo_2Al_8$  is also a strong easy-axis AFM material. Moreover, we show that the  $PrCo_2Al_8$  undergoes two consecutive AFM transitions. For both materials, applying a magnetic field ( $H$ ) along the  $c$ -axis induces metamagnetic transitions from the AFM state to a high field polarized paramagnetic phase state at relatively low  $H$ . The  $T$  vs.  $H$  phase diagrams for the samples are constructed based upon magnetization ( $M(H, T)$ ) measurements. The Sm-based material was previously described as a Pauli paramagnet (where Sm would assume a 2+ valence) [32]. Here, we show that it is a moment bearing compound with an AFM transition,  $T_N \approx 22$  K.

## II. METHODS

Motivated by previous work [32],  $RCo_2Al_8$  single crystals ( $R = La, Ce, Pr, Nd$  and  $Sm$ ) were obtained from an Al-rich ternary composition (1 : 2 : 20). A total amount of about 3.5 g of reactants were weighted and placed in Canfield crucible set (CCS) [34, 35]. Guided by the methods explained elsewhere [34], the heat treatment was slightly modified to obtain phase pure single crystals: from room temperature ( $RT$ ), the reactants were heated for 6 hours to  $T = 1180$  °C. The mixture was left at this temperature for 24 hours and then slowly

cooled down to  $T = 900$  °C at a rate of 2 °C/h, at which point the growth was taken out of the furnace and spun to segregate the flux from the crystals. The samples thus obtained were rod-like in shape with typical size about 2-3 mm in length with a cross section of about  $1 \times 1$  mm. Larger crystals, about 1 cm in length (see inset in figure 1(b)), could be obtained by either of the two methods: *i*) cooling down the melt from  $T = 1180$  °C at a slower rate of 1 °C/h or by *ii*) growing the crystals in a two step process; first cooling the melt to 1025 °C and decanting, which promotes the removal of any oxide slags that can serve as unwanted nucleation sites. This makes the solution more pure. Then, secondly, taking the materials that were decanted at 1025 °C, resealing and heating to 1100 °C and cooling to 900 °C over 150 hours.

We have observed that when attempting to grow  $RCo_2Al_8$  single crystals with heavier lanthanides (Gd - Tm), we obtained a new phase:  $R_2Co_6Al_{19}$  whose preparation and detailed physical properties will be the subject of a separate report. Indeed, as exemplified by phases containing Ce-Co-Al, Pr-Co-Al and Nd-Co-Al [36–38], many ternary  $R$ -Co-Al phases are possible.

Pieces of the obtained samples were selected, crushed and passed to a 90  $\mu$ m sieved to obtain a fine powder to perform powder x-ray diffraction (XRD) experiments. A commercial table top Rigaku Miniflex X-ray diffractometer was employed for the XRD experiments. The GSAS2 software [39] was used to analyze the powder profile and check the crystallographic phase. The crystal orientation was checked by Laue diffraction experiments. We could clearly distinguish the crystallographic  $c$ -axis (the axis along the rod length) but not the  $a$  and  $b$  axes, due to the formation of twins in the  $ab$  plane. As a consequence of this, all anisotropic data is given only as parallel to the identified  $c$ -axis and perpendicular to the identified  $c$ -axis. This means that we are not able to study any possible in-plane anisotropy in this system.

Magnetization ( $M$ ) measurements (as function of  $H$  and  $T$ ,  $M(H)$  and  $M(T)$ , respectively) were performed in commercial SQUID magnetometers from Quantum Design. Measurements were performed down to  $T = 1.8$  K and fields as high as  $\mu_0 H = 7$  T. Experiments were performed with the applied field either along the  $c$ -axis (denoted  $H \parallel c$ ) or perpendicular to the  $c$ -axis directions (denoted  $H \perp c$ ). For all samples, zero field cooling (ZFC) and field cooling (FC)  $M(T)$  measurements were performed and no notable differences were found. In this paper, we present the ZFC measurements.

Heat capacity,  $C_p(T)$ , and electrical transport measurements were performed in a commercial Dynacool Physical Property Measurement System (PPMS) from Quantum Design. In the case of the La- and Ce-based system, the electrical transport was characterized adopting two configurations, namely the current parallel and perpendicular to the  $c$ -axis (denoted  $\rho_c$  and  $\rho_{ab}$ , respectively). For the other  $R$ -based materials, the electrical transport was characterized only for the current parallel to the  $c$ -axis.

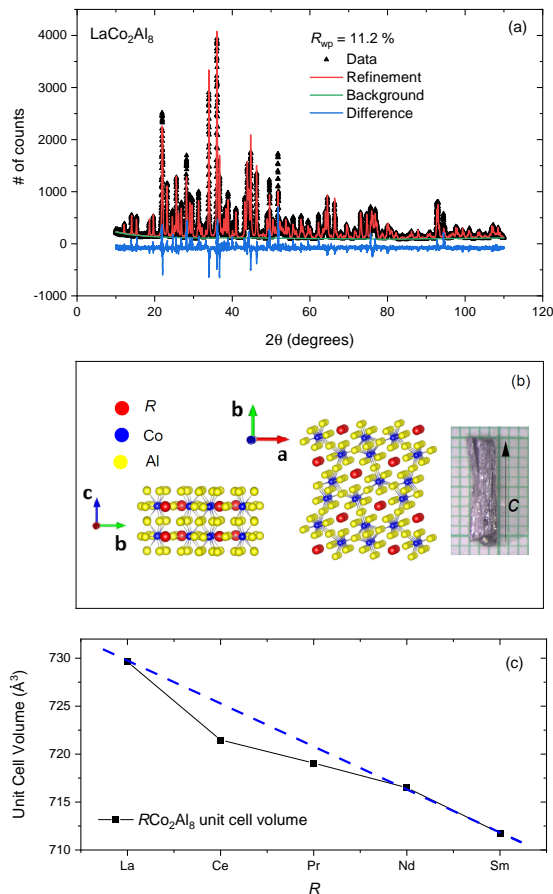


Figure 1. (a) Black-squares:  $\text{LaCo}_2\text{Al}_8$  powder XRD experimental data, respective powder profile refinement (thick red line), background fitting (thick green line) and difference pattern (thick blue line) obtained with a  $R_{\text{WP}} \approx 11.2\%$ . (b) Structural model of the  $\text{CaCo}_2\text{Al}_8$ -type orthorhombic crystal structure (space group  $Pbam$ ).  $R$  atoms are represented by red spheres, Co atoms by blue spheres and the Al atoms yellow spheres. Some key structural features are highlighted by the model: *i*) the  $R$ -chains along the  $c$ -axis and the skewed triangular lattice in  $ab$ -plane formed by the  $R$  atoms *ii*) the Co coordination structure by the Al atoms and *iii*) the cage-like structure around the  $R$  sites. In the inset, we show a large  $\text{CeCo}_2\text{Al}_8$  single crystal (see methods), about 1 cm in length along the  $c$ -axis. (c) Unit cell volume of the  $R\text{Co}_2\text{Al}_8$  materials as function of  $R$ , as obtained by Rietveld refinement of the powder XRD data (typical  $R_{\text{WP}} \approx 11.0 - 12.0\%$ , error bars are of the order of the point size).

### III. RESULTS AND DISCUSSION

#### A. Crystal structure and $\text{LaCo}_2\text{Al}_8$ physical properties

Powder XRD data were collected for all  $R\text{Co}_2\text{Al}_8$  ( $R = \text{La, Ce, Pr, Nd and Sm}$ ) materials. The resulting diffraction patterns were refined assuming the previously reported data from single crystal diffraction experiments

[32] (space group  $Pbam$ ), providing a good description of experimental data. The lattice constants assume typical values as  $c \sim 4.0$  Å,  $a \sim 12.0$  Å and  $b \sim 14.0$  Å. Figure 1(a) present the  $\text{LaCo}_2\text{Al}_8$  powder XRD data (black circles) and refinement results (red and blue thick lines). The quality of the data analysis is representative of the series.

In figure 1(b), the refined structure is represented. Focusing first on the structural features related to the  $R$  atoms (red spheres), it can be observed that along the  $c$ -axis the  $R$  atoms are organized along somewhat isolated chains. The model also highlights the cage-like structure formed around the  $R$  site, which is reminiscent of what is found in intermetallic cage-like materials. Considering the structure projected in the  $ab$  plane, the sublattice formed by the  $R$  atoms is a motif containing skewed triangles for which AFM interactions might be somewhat frustrated. The Co-Al polyhedra show that there is no direct  $R$ -Co contacts, and thus the role of the hybridization between the  $R$ -derived orbitals and the Co-derived  $3d$  orbitals is negligible. The Co atoms are coordinated by 9 Al atoms and the typical Co-Al distances are less than the sum of the Co and Al metallic radii, suggesting a significant covalent character of the Co-Al bond. This feature weakens the Co magnetism, as is demonstrated by the Pauli-paramagnetism of the  $\text{LaCo}_2\text{Al}_8$  crystal shown in Fig. 2(a). Thus,  $R\text{Co}_2\text{Al}_8$  magnetic properties are dominated by those of the trivalent  $R$ -ions.

Figure 1(c) shows the unit cell volume, obtained from the powder XRD refinement along the series, and the results are in good agreement with the single crystal refinement [32]. Whereas there is a clear Lanthanide contraction, the unit cell for  $\text{CeCo}_2\text{Al}_8$  appears to be somewhat lower than would be expected, suggesting some possible degree of tetravalent nature, or perhaps more accurately, some degree of hybridization.

Assuming the partitioning of the electronic (localized  $4f$  electrons plus conduction electrons) and lattice degrees of freedom of the other  $R\text{Co}_2\text{Al}_8$  materials,  $\text{LaCo}_2\text{Al}_8$  can thus be rationalized as a suitable reference material to obtain the  $4f$ -electron contributions to physical properties of the other  $R$ -based materials. We thus investigate the  $\text{LaCo}_2\text{Al}_8$  magnetization, electrical transport and heat capacity ( $C_p$ ). Turning to measurements of physical properties, Fig. 2(a) presents data on the  $\text{LaCo}_2\text{Al}_8$  single crystalline sample. The  $\text{LaCo}_2\text{Al}_8$  magnetization  $M$  as function of  $T$ , obtained with an applied field  $\mu_0 H$  of 0.1 T, is presented in figure 2(a). We define the system susceptibility,  $\chi$ , as  $M/H$ . The results are nearly  $T$ -independent, as expected for a Pauli paramagnet, and the observed value is  $\approx 2 \times 10^{-4}$  emu/mol.Oe.

Resistivity ( $\rho$ ) measurements (current  $\parallel c$ -axis and  $\parallel ab$ -plane, denoted as  $\rho_c$  and  $\rho_{ab}$ , respectively) are presented in 2(b) for  $2 < T < 300$  K. Metallic behavior with residual resistivities of about  $\rho_c \approx 8 - 10$   $\mu\Omega\cdot\text{cm}$  and  $\rho_{ab} \approx 40 - 55$   $\mu\Omega\cdot\text{cm}$  are observed at  $T = 2$  K. Similarly, a factor in between  $\approx 4 - 7$  is observed for  $\rho_{ab}/\rho_c$  at  $T = 300$  K, characterizing a strong electronic anisotropy.

Room temperature resistivity ratio ( $RRR$ ) parameters between  $\approx 5 - 6$  were obtained, similar to what we observed for the other  $R$ -based materials. Resistivity measurements were performed for 3 samples ( $\rho_c$ ) and 2 samples ( $\rho_{ab}$ ), each with its own error bar. In the former case, typical dimensions for the distance between the electrodes ( $L$ ) were  $\approx 0.8 - 1.1$  mm and the cross section area ( $A$ ) were in between  $\approx 0.18 - 0.20$  mm<sup>2</sup>. In the latter case, measurements were executed with values in between  $L \approx 0.4 - 0.6$  mm and  $A \approx 0.25 - 0.30$  mm<sup>2</sup>. For  $\rho_{ab}$ , the actual measurements differ by a factor of about  $\approx 1.6$  and we also present the average between the two curves to be inspected in reference with the estimated error bars.

The  $C_p$  data as function of  $T$  are presented in Fig. 2(c). From now on, we shall denote by  $C_p^R$  the heat capacity of the  $R$ -based material. No sign of a phase transition was observed down to  $T = 1.81$  K, as previously reported [29]. The  $C_p^{La}$  data assume an almost constant value in the low- $T$  region. Indeed, in the simplest approximations, it is expected that  $C_p$  at sufficient low- $T$  should be modeled as  $C_p/T = \gamma + \beta T^2$ , where  $\gamma$  is the Sommerfeld coefficient, connected with the conduction electrons and  $\beta$  is a constant connected with the Debye (phonon) contributions to  $C_p$ . The adequacy of this model is investigated in the upper inset of the figure wherein we plot  $C_p^{La}/T^3$  as a function of  $T$ .

A broad peak at about 25 K is observed. Such contribution is reminiscent of a low frequency non-dispersive phonon, usually paraphrased as a “rattling mode” of the  $R$  atoms inside a cage-like structure. This vibration is connected with good potential for thermoelectric applications in cage-like materials such as skutterudites and clathrates [40–43]. These modes are modeled, in first approximation, by an Einstein contribution to the heat capacity which contains a single parameter: the Einstein temperature  $\Theta_E$ . A peak about 25 K in the heat capacity data is associated with  $\Theta_E \approx 125$  K. Whereas this number stands out as a rather low-frequency optical vibration, vibrations as low as  $\approx 1$  GHz ( $\approx 5$  K) were already characterized for rattlers in skutterudite materials [44].

Figure 2(d) plots  $C/T$  versus  $T^2$  for  $0 < T^2 < 30$  K. Whereas the data for  $T^2 < 25$  K is well approximated by the Debye model with  $\gamma^{La} \approx 18.2(5)$  mJ/mol.K<sup>2</sup> and  $\beta^{La} \approx 0.45(2)$  mJ/mol.K<sup>2</sup>, for  $T^2 > 25$  this is not the case. This is most likely associated with the low-lying Einstein mode discussed above.

The  $\gamma^{La}$  was obtained per mol of formula unit and it is then close to  $\approx 1.5$  mJ/mol.K<sup>2</sup> per atom, as expected for simple metals, i.e., our estimate for  $\gamma^{La}$  does not suggest enhancement of the quasiparticle mass. Indeed, the ratio between the Pauli-like response and  $\gamma^{La}$  ( $2 \times 10^{-4}/\gamma^{La}$  emu.K<sup>2</sup>/mJ) is  $\approx 1.24 \times 10^5$  (emu.K<sup>2</sup>/mJ) close to  $1.37148 \times 10^5$  (emu.K<sup>2</sup>/mJ) deduced for a simple free electron gas [45]. Overall, LaCo<sub>2</sub>Al<sub>8</sub> is a Pauli paramagnet that can be adopted as a “non-magnetic” reference material for the  $R$ Co<sub>2</sub>Al<sub>8</sub> ( $R = \text{Ce, Pr, Nd and Sm}$ ) compounds. This said, we should note three impor-

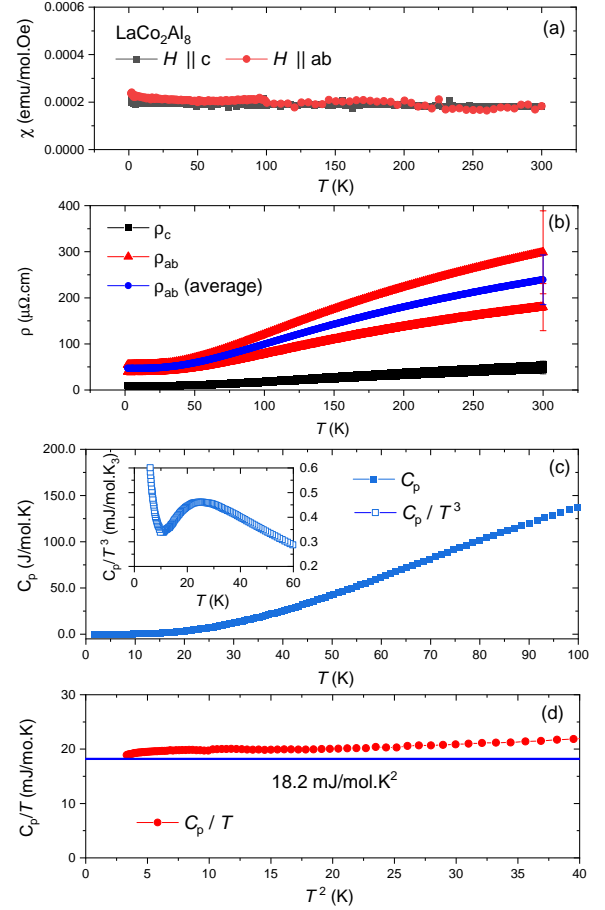


Figure 2. LaCo<sub>2</sub>Al<sub>8</sub> physical properties. (a)  $\chi$  as a function of  $T$  obtained for  $\mu_0 H = 0.1$  T, for  $H$  along the  $c$ -axis ( $H \parallel c$ ) and in the  $ab$  plane ( $H \parallel ab$ ). (b)  $\rho_c$  and  $\rho_{ab}$  as a function of  $T$ , in the interval  $2 < T < 300$  K. (c)  $C_p$  as function of  $T$ . The inset presents  $C_p/T^3$  as function of  $T$ , which displays a broad peak about  $T = 25$  K (see main text). (d)  $C_p/T$  as a function of  $T^2$  in a limited  $T$ -range. A reference line (solid blue line) marks the extrapolated value of  $C_p/T$  as  $T \rightarrow 0$ .

tant points. First, similar Einstein modes should exist for the other ( $R = \text{Ce, Pr, Nd, and Sm}$ ) members of the  $R$ Co<sub>2</sub>Al<sub>8</sub> family. We do not know the exact value of their Einstein temperatures, but given the lanthanide contraction, it will probably shift in some monotonic manner. Second, even with this uncertainty, the LaCo<sub>2</sub>Al<sub>8</sub>  $C_p$  data remain a good non-magnetic analogue for subtraction from the other  $R$ Co<sub>2</sub>Al<sub>8</sub> materials because even with a possible small shift in Einstein temperature, the total entropy change over a wide temperature range will be well modeled by the LaCo<sub>2</sub>Al<sub>8</sub>. Third, as such, we will not be able to use the typical low- $T$  heat capacity model to extract values for  $\gamma$  and  $\beta$  for the other  $R$ Co<sub>2</sub>Al<sub>8</sub> compounds.



## B. The Kondo lattice $\text{CeCo}_2\text{Al}_8$

In figures 3(a)-(c) the magnetic properties of  $\text{CeCo}_2\text{Al}_8$  are presented. Magnetization measurements were made for  $\mu_0 H = 0.1$  T, for  $H \parallel c$  and  $H \parallel ab$ . In 3(a),  $\chi$  is presented and the magnetic response is clearly anisotropic, with the  $c$ -axis being the easy axis of magnetization. As aforementioned, twins were observed in the  $ab$  plane and therefore measured quantities for which  $H \parallel ab$  are, to a certain approximation, averages between results expected with  $H \parallel a$  or  $b$ . From now on we identify quantities obtained in measurements with  $H$  either parallel to  $c$  or to  $ab$  by their respective subscripts. When necessary, we shall also adopt a label  $R$  to denote a quantity associated to the  $R$ -based material.

A Curie-Weiss (CW) like behavior is observed for  $\chi_c$  down to  $T \approx 15$  K, below which a tendency for saturation is observed. This is reminiscent of the formation of an enhanced Pauli-like response of coherent heavy carriers (contributed by the Ce  $4f$  states) in Kondo-lattice systems. Along the  $ab$ -plane,  $\chi_{ab}$  has a weaker  $T$ -dependence and it also tends to saturate at low- $T$ . In the inset of 3(a), we present the inverse of  $\chi_c$  and  $\chi_{ab}$  subtracted by  $\chi_0 = 2 \times 10^{-4}$  emu/mol.Oe which is the  $\text{LaCo}_2\text{Al}_8$  Pauli-like response. We then fit the data (in the  $T > 150$  K region) to a inverse CW expression to obtain the Curie-Weiss constants  $\theta_c^{\text{Ce}} = -1.6(5)$  K and  $\theta_{ab}^{\text{Ce}} = -267(4)$  K.

To estimate the effective moments and the energy scale of the interactions, we adopt a CW description of the polycrystalline average of  $\chi$ , denoted by  $\chi_{\text{ave}}$ . Assuming that  $\chi_{ab}$  is an average between  $\chi_a$  and  $\chi_b$ , we define  $\chi_{\text{ave}}$  as  $\chi_{\text{ave}} = (\chi_c + 2\chi_{ab})/3$ . In figure 3(b), we present  $\chi_{\text{ave}}$  (left axis) and  $(\chi_{\text{ave}} - \chi_0)^{-1}$  (right axis). We performed the CW fitting of  $(\chi_{\text{ave}} - \chi_0)^{-1}$  (for  $T > 150$  K) and obtained  $\mu_{\text{eff}}^{\text{Ce}} = 2.43(1) \mu_B$  and  $\theta_{\text{CW}}^{\text{Ce}} = -68(2)$ . The value of  $\mu_{\text{eff}}^{\text{Ce}}$  corresponds to 0.96 of the full value expected for the  $\text{Ce}^{3+}$  cations ( $2.57 \mu_B$ ), suggesting that the Ce derived moments are well localized in the  $T > 150$  K region. Being negative,  $\theta_{\text{CW}}^{\text{Ce}}$  suggests AFM interactions.

For both directions, there is a clear upturn in  $\chi$  at low- $T$ , that may suggest a paramagnetic impurity in the sample or the onset of magnetic order. This is further investigated by isothermal magnetization measurements at  $T = 1.81$  K,  $H \parallel c$  and  $H \parallel ab$ , presented in the inset of Fig. 3(a). The results clearly suggest that the system is not magnetically ordered at this temperature.

Motivated by the anisotropy of  $\text{CeCo}_2\text{Ga}_8$  electronic properties and the proposal of an axial Kondo lattice in the material, we measured  $\rho^{\text{Ce}}$  with the current parallel and perpendicular to the  $c$ -axis. In figure 3(d),  $\rho_c$  and  $\rho_{ab}$  for the Ce-based material are presented. As is observed,  $\rho^{\text{Ce}}$  is also marked by a significant anisotropy and by broad maximums suggesting the formation of a Kondo lattice. At  $T = 300$  K,  $\rho_{ab}/\rho_c$  is about 5. We applied the same procedure used for the La samples to the Ce samples. The resistivity was measured in both directions across multiple single crystals as shown in the

figure.

As a way estimate the contribution of the Ce derived  $4f$  states to the  $\text{CeCo}_2\text{Al}_8$  transport properties, we show in 3(e)  $\rho_{4f}^{\text{Ce}} = \rho^{\text{Ce}} - \rho^{\text{La}}$ . For better comparison, we magnify the  $\rho_c$  data multiplying it by a factor of 3 as indicated in the figure. The  $\rho_{4f}^{\text{Ce}}$  curves were obtained from the averages of the  $\rho^{\text{Ce}}$  and  $\rho^{\text{La}}$  presented in figures 3(d) and 2(b), respectively. Broad resistivity maximums are observed at clearly distinct positions, based upon which we define anisotropic Kondo coherence temperatures ( $T_K^*$ ) of about  $T_{K,c}^* \approx 68$  K and  $T_{K,ab}^* \approx 46$  K. Our findings suggest the emergency of anisotropic heavy quasi particles due to formation of a Kondo lattice in  $\text{CeCo}_2\text{Al}_8$ . The  $RRR$  obtained for  $\text{CeCo}_2\text{Al}_8$  is about  $\approx 5$ , similar to the  $\text{LaCo}_2\text{Al}_8$  case (see figure 2(b)). By inspection, one observes that  $\rho_{\text{Ce},ab}$  is about 5 times  $\rho_{\text{Ce},c}$  at  $T = 300$  K.

Electronic correlations and the presence of heavy carriers are further investigated in figures 3(f)-(g), where we present the  $\text{CeCo}_2\text{Al}_8$  specific heat data and analysis. In figure 3(f), the  $\text{CeCo}_2\text{Al}_8$   $C_p$  data is presented alongside those of  $\text{LaCo}_2\text{Al}_8$ . No sign of a phase transition is observed down to  $T = 1.81$  K, as previously reported [29]. In comparison with the La-based material, a systematic and clear entropy excess in the Ce-based system is observed, in particular in the low- $T$  region. In the inset,  $C_p/T$  data are presented as function of  $T^2$ , for both materials. A clear upturn, reminiscent of a Kondo system, possibly close to quantum criticality, is observed in  $C_p^{\text{Ce}}$  at low- $T$  as previously observed in the case of polycrystalline samples [29]. We can estimate the low temperature  $\gamma^{\text{Ce}}$  as being between  $173(3)$  mJ/mol.K<sup>2</sup> (from the extrapolation of the linear part of  $C_p/T$  vs.  $T^2$  to zero) and  $337(5)$  mJ/mol.K<sup>2</sup> (from the lowest temperature value measured). As such,  $\text{CeCo}_2\text{Al}_8$  is a moderate heavy Kondo lattice system.

Having in mind the caveat related with the presence of the low-lying optical phonon in  $\text{LaCo}_2\text{Al}_8$ , we examine an estimate for the  $\text{CeCo}_2\text{Al}_8$  magnetic heat capacity, which we obtain from  $C_{\text{mag}}^{\text{Ce}} = C_p^{\text{Ce}} - C_p^{\text{La}}$ . We then integrate  $C_{\text{mag}}^{\text{Ce}}/T$  to calculate the magnetic contribution to the  $\text{CeCo}_2\text{Al}_8$  entropy variation  $\Delta S$  up to 300 K. This is presented in figure 3(f). As observed,  $\Delta S$  only shows a tendency for saturation at high- $T$  and the saturation value is about  $R \times \ln(4)$  only close to 300 K. If we take one of the conventional estimates of the thermodynamic Kondo temperature ( $T_K$ ), namely when magnetic entropy reaches  $R \times \ln(2)$ , we can estimate  $T_K \approx 36$  K.

For an alternate estimate of  $T_K$ , one can inspect the inset of 3(e) and conclude that  $C_{\text{mag}}^{\text{Ce}}$  is underestimated for  $T < 1.81$  K, because of the  $C_p^{\text{Ce}}$  upturn in this region. It is then likely that an entropy amounting to  $R \times \ln(4)$  is recovered for  $T < 300$  K. Thus, by adopting the generalized relation  $\gamma^{\text{Ce}} T_K = R \times \ln(4)$  [14] one finds  $T_K \approx 70$  K, in good agreement with  $T_{K,c}^*$ . This expression assumes that two low-lying CF doublets hybridize to form the Kondo state.

From our experiments and analysis, one can deduce the formation of a coherent Kondo lattice featuring moder-

ate heavy quasi-particles in  $\text{CeCo}_2\text{Al}_8$ . The electronic and magnetic properties of the system are anisotropic and, most strikingly, the deduced Kondo coherence temperatures are anisotropic, with a difference of about 22 K between  $T_{K,c}^*$  and  $T_{K,ab}^*$ . Our findings support a scenario wherein Kondo coherent scattering is first achieved along the  $c$ -axis whereas in a relatively broad  $T$ -interval the Kondo scattering in the  $ab$  plane remains incoherent, reminiscent of the single ion Kondo effect. Moreover, in view of our results for  $\text{LaCo}_2\text{Al}_8$ , the Kondo anisotropy in  $\text{CeCo}_2\text{Al}_8$  is likely an effect that derives from the conduction electrons, not necessarily related with the local hybridizations.

There is no clear *qualitative* difference between  $\text{CeCo}_2\text{Al}_8$  and  $\text{CeCo}_2\text{Ga}_8$ . The materials are isoelectronic and the structural parameters are in close similarity, which renders similar Ce-Ga and Ce-Al distances. Sample quality, as determined from  $RRR$ , is also similar. Moreover, the resistivity anisotropy at 300 K is also comparable [24, 26]. In  $\text{CeCo}_2\text{Ga}_8$ ,  $\rho_c$  peaks about 17 K whereas no coherence peak is observed for either  $\rho_a$  or  $\rho_b$  down to 2 K. This, and results from optical spectroscopy experiments, supports the proposal of an axial Kondo chain in this material [25, 26]. In view of our findings for  $\text{CeCo}_2\text{Al}_8$ , it is possible that a coherence peak in  $\rho_a$  and  $\rho_b$  may exist also in  $\text{CeCo}_2\text{Ga}_8$ , but is delayed to lower temperatures. The synthesis of  $\text{LaCo}_2\text{Ga}_8$  single crystal and the investigation of its transport properties is certainly highly desirable to understand how analogous the situation is.

### C. $\text{PrCo}_2\text{Al}_8$ and $\text{NdCo}_2\text{Al}_8$

We now inspect, in turn, the Pr- and Nd-based materials. We start with the former.  $\chi$  measurements (figure 4(a)) display our key findings about this material: it is a strong easy-axis magnet presenting AFM order. From the  $H \parallel c$  data, a Neel temperature ( $T_N$ ) of  $T_N = 4.84$  K can be deduced. In the inset, this subject is investigated in detail. We present high statistics measurements for  $d(T\chi_c)/dT$  about  $T_N = 4.84$  K, which adds some complexity to our findings. The data display two putative AFM transitions, which we shall call AFM phase *I* and *II*, taking place at  $T_{N1} = 4.84$  K and  $T_{N2} = 4.71$  K, respectively. Multiple magnetic transitions were also observed in other orthorhombic Pr-Co-Al ternaries, such as  $\text{PrCoAl}_4$  [37, 46, 47].

In figure 4(b) we analyze the inverse of  $\chi_c$  and  $\chi_{ab}$ . As recently reported for this same material [28] and other Pr-based materials adopting the  $\text{CaCo}_2\text{Al}_8$ -type structure [27, 31],  $\chi_{ab}^{-1}$  deviates strongly from the expected CW behavior. This deviation was attributed to excited CF levels lying about this energy scale. In figure 4(a), close inspection shows that indeed  $\chi_{ab}$  has a broad peak-like structure (a “belly”), suggesting that only data in the high- $T$  region should be considered for CW fittings. We then perform the inverse CW fitting for  $T > 225$  K

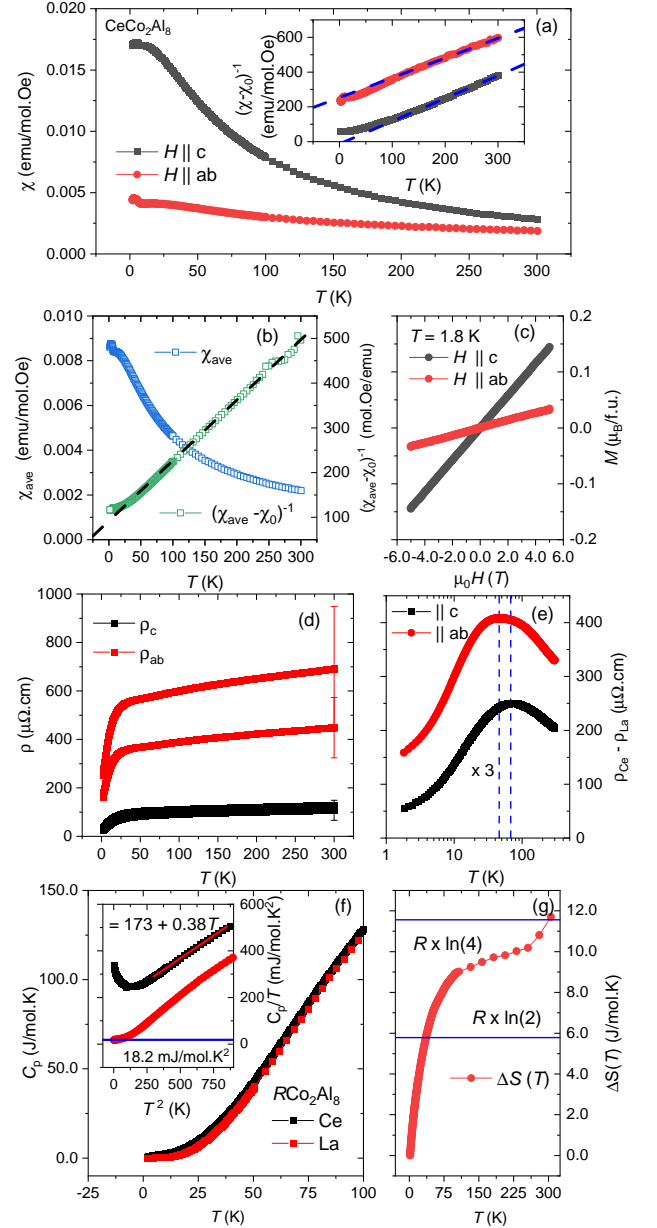


Figure 3.  $\text{CeCo}_2\text{Al}_8$  physical properties. (a) The  $\text{CeCo}_2\text{Al}_8$   $\chi_c$  and  $\chi_{ab}$ . In the inset, we present the inverse of  $(\chi_{ab} - \chi_{ab0})$  and  $(\chi_c - \chi_{c0})$ . The dashed blue lines represent the CW fitting (obtained for  $T > 150$  K) of the data. (b) Respectively on the left and right axis,  $\chi_{\text{ave}}$  and  $(\chi_{\text{ave}} - \chi_0)^{-1}$  are presented. The dashed black line represents the inverse CW fitting of the data (obtained for  $T > 150$  K). (c) Isothermal magnetizations obtained for  $H \parallel c$  and  $H \parallel ab$  at  $T = 1.8$  K. (d)  $\text{CeCo}_2\text{Al}_8$   $\rho_c$  and  $\rho_{ab}$  as a function of  $T$  for a number of single crystals. (e) The Ce 4f contribution to resistivity ( $\rho_{4f,Ce} = \rho_{Ce} - \rho_{La}$ ) as a function of  $T$  in a log scale, for the two different directions. The vertical blue line marks the maximums of  $\rho_{4f,Ce}$  which we adopt as an estimate to  $T_{K,c}^* = 68$  K and  $T_{K,ab}^* = 46$  K. Note that average values of the respective resistivity curves were used. (f)  $\text{CeCo}_2\text{Al}_8$  and  $\text{LaCo}_2\text{Al}_8$  heat capacity. The inset shows in detail the  $C_p$  vs.  $T^2$  at low- $T$ . (g) The magnetic entropy contribution ( $\Delta S$ ) of  $\text{CeCo}_2\text{Al}_8$  and some reference values (solid blue lines).

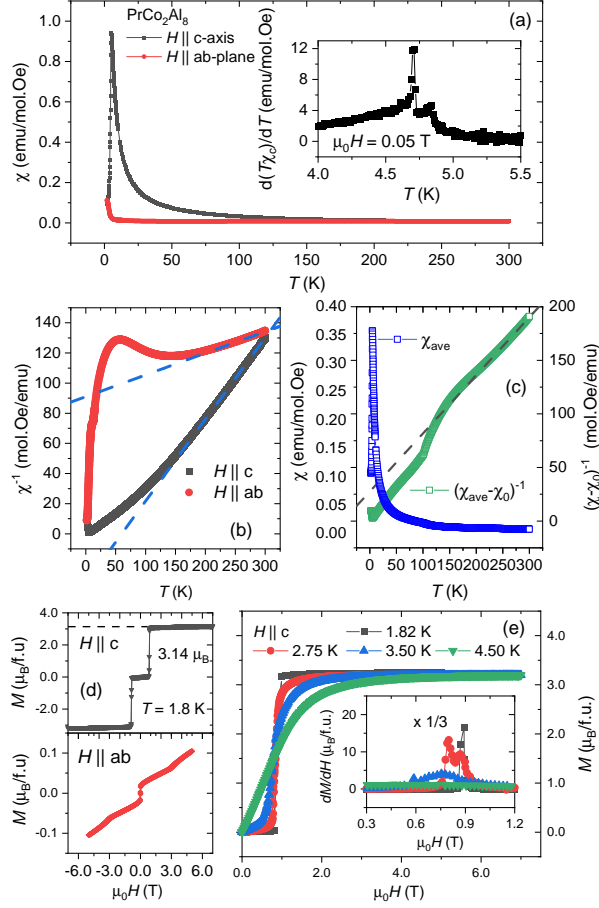


Figure 4.  $\text{PrCo}_2\text{Al}_8$  magnetic properties. (a)  $\chi$  data obtained for  $\mu_0 H = 0.1$  T with  $H \parallel c$  and  $H \parallel ab$ . Strong easy axis anisotropy is observed. The measurement with  $H$  along the  $c$ -axis suggest an AFM transition at  $T_N = 4.84$  K. The inset shows in detail the behavior of  $d(T\chi)/dT$  close to the transition temperature and two transitions are observed ( $T_{N1} = 4.84$  K and  $T_{N2} = 4.71$  K). (b) The inverse of  $\chi_a$  and  $\chi_{ab}$  subtracted by  $\chi_0$ . The dashed blue lines represent the CW fitting (obtained for  $T > 225$  K) of the data. (c) Respectively on the left and right axis,  $\chi_{\text{ave}}$  and  $(\chi_{\text{ave}} - \chi_0)^{-1}$  are presented. The solid black line represent the inverse CW fitting of the data ( $T > 225$  K). (d) Isothermal magnetization curves ( $T = 1.81$  K) obtained with  $H \parallel c$  (upper panel) and  $H \parallel ab$  (lower panel). (e) Representative isothermal magnetizations for distinct temperatures obtained with  $H \parallel c$ . The data show clear metamagnetic transitions from a low field AFM state to a high field spin polarized PM phase. The inset shows the  $dM/d\mu_0 H$  derivatives from which we determine the critical field for the field-induced metamagnetic transition. The inset also shows that at some intermediate  $T$  two inflections are observed in  $dM/d\mu_0 H$ .

obtaining  $\theta_c = 59(3)$  K and  $\theta_{ab} = -631(10)$  K.

In figure 4(c), left axis, we present  $\chi_{\text{ave}}$ . To estimate  $\mu_{\text{eff}}^{\text{Pr}}$  and  $\theta_{\text{CW}}^{\text{Pr}}$ , we first noticed that  $1/\chi_{\text{ave}}$  contains a clear deviation from linear behavior. This is most likely a manifestation of the fact that we are not performing a proper polycrystalline average but rather using  $\chi_{ab}$  as a proxy for the, average, in-plane susceptibility. The fact that we still see a CEF feature in our polycrystalline average suggests that there is actually sizable in-plane magnetic anisotropy. We thus adopted a CW fitting only in the  $T > 225$  K region and use the fitting to extract a constant paramagnetic contribution  $\chi_0$  which, due to a Vlan Vleck term, is not the same as the  $\text{LaCo}_2\text{Al}_8$  contribution. Then, the linear CW fitting of the  $(\chi_{\text{ave}} - \chi_0)^{-1}$  data was performed again in the restricted  $T > 225$  K region. This is shown in the right axis of figure 4(c) and the fitting is represented by the black dashed line. Based on this procedure,  $\mu_{\text{eff}}^{\text{Pr}} = 3.82(5) \mu_B$  and  $\theta_{\text{CW}}^{\text{Pr}} = -47(2)$  K are estimated. The effective moments are very close to the theoretical value for  $\text{Pr}^{3+}$  cations ( $3.57 \mu_B$ ) but is an overestimation. From  $\theta_{\text{CW}}^{\text{Pr}}$ , a large frustration parameter  $f = |\theta_{\text{CW}}^{\text{Pr}}/T_N| \approx 10$  is deduced. The  $\mu_{\text{eff}}^{\text{Pr}}$  value may indicate some contribution from Co, that may become magnetically polarized due to the Pr presence. It has to be noted, though, given the fact that the polycrystalline average data so clearly violates CW-behavior, our values of  $\theta_{\text{CW}}^{\text{Pr}}$  and  $\mu_{\text{eff}}^{\text{Pr}}$  should be viewed as more qualitative than quantitative.

The properties of the AFM state are further investigated by isothermal magnetization measurements. Results at  $T = 1.81$  K, for  $H \parallel c$  (upper panel) and  $H \parallel ab$  (lower panel) are presented in figure 4(d). A metamagnetic transition from a low field AFM state to a high field spin-polarized paramagnetic (PM) state is observed at about  $\approx 0.9$  T for  $H \parallel c$ . The saturation value is  $\approx 3.14 \mu_B/\text{f.u.}$  very close to what is expected for a  $\parallel 4$  singlet CF ground state. Indeed, in the case of  $\text{Pr}^{3+}$  cations, which are non-Kramers ( $J = 4$ ), the degeneracy of the CF levels can be completely removed. In the case of  $\text{PrCo}_2\text{Al}_8$ , in view of the low Pr point group symmetry ( $m2$ ), the CF scheme should feature only singlets and doublets and possibly pseudo-doublets, which denote two nearby singlets.

For  $H \parallel ab$ , a spin rotation transition is observed and induced by a relatively small field. By comparing the values of the magnetization at 1.81 K and  $\mu_0 H = 5$  T for the two field directions, the magnetic anisotropy in  $\text{PrCo}_2\text{Al}_8$  is about  $\approx 32$ .

In figure 4(e), we explore the temperature dependence of the metamagnetic transition, presenting some representative isothermal magnetization curves, obtained for  $H \parallel c$ , in the interval  $1.81 < T < 5$  K. In the inset, we show the field derivative of the isothermal magnetization ( $dM/d\mu_0 H$ ). We adopt that a peak in the derivative identify the critical field at which the metamagnetic transition takes place. As can be observed, above the base temperature (for instance for  $T = 2.75$  K, red circles in 4(e)), the saturation moment is reached after two peaks

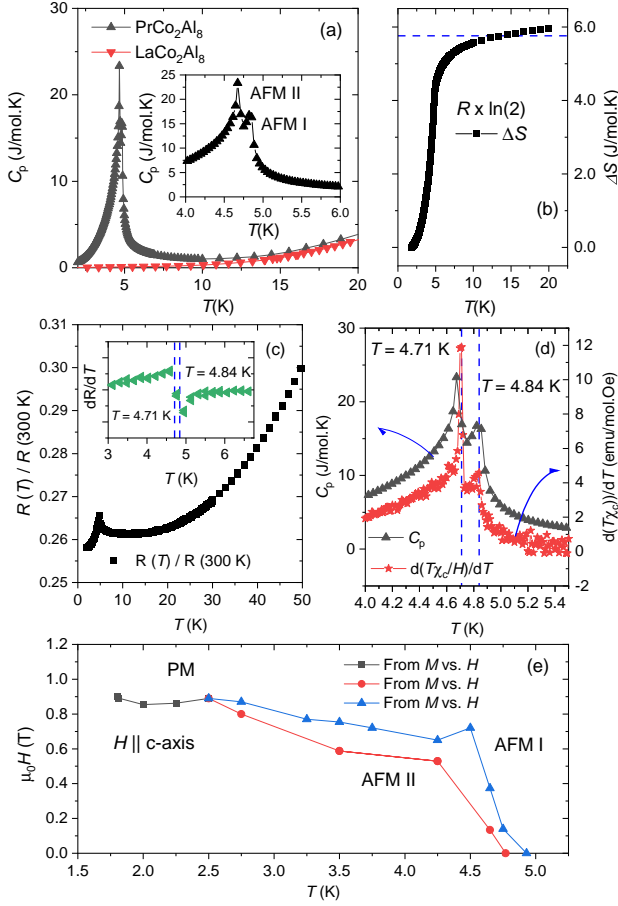


Figure 5. PrCo<sub>2</sub>Al<sub>8</sub> thermal and transport properties. (a) PrCo<sub>2</sub>Al<sub>8</sub>  $C_p$  (black triangles) showing the AFM transitions. The inset provide detail data in the vicinity of  $T_N$  and show the two consecutive transitions which are also observed in the  $\chi$  measurements. The LaCo<sub>2</sub>Al<sub>8</sub>  $C_p$  is presented as reference. (b) PrCo<sub>2</sub>Al<sub>8</sub> magnetic entropy variation (see main text). (c) Temperature dependence of the normalized resistance  $R(T)/R(300 K)$ . The inset shows the resistance derivative to  $T_{N1,2}$ . (d) Comparison between  $C_p$  and  $d(T\chi_c)/dT$  showcasing the two AFM transitions as determined from independent measurements. (e) PrCo<sub>2</sub>Al<sub>8</sub> magnetic phase diagram ( $H \parallel c$ ) deduced from  $M(H)$  measurements.

of the derivative. We associate the low-field peak with a transition from AFM II to AFM I and the second peak with a transition to the high field spin polarized PM phase. For low- $T$  measurements ( $T \leq 2.5$  K), only one critical field is observed. We thus conclude that at a certain  $T$  and  $H$ , the transitions to the AFM I and II phases coalesce in a single transition line (see Fig. 5(f)).

The PrCo<sub>2</sub>Al<sub>8</sub>  $C_p$  (denoted  $C_p^{\text{Pr}}$ ) is presented in figure 5(a) alongside the LaCo<sub>2</sub>Al<sub>8</sub> reference data. The inset shows  $C_p^{\text{Pr}}$  in detail the vicinity of the values of the putative AFM transition temperatures. It clearly shows the two transitions at  $T_{N1} = 4.84$  K and  $T_{N2} = 4.71$  K.

We investigate the total entropy associated with the magnetic ordering in 5(b). In all cases, the magnetic en-

tropy is estimated by adopting  $C_p^{\text{La}}$  plus a renormalization factor which accounts the mass difference between La and the relevant  $R$  atom. This renormalization factor is  $\Theta_D^R/\Theta_D^{\text{La}}$  where  $\Theta_D^R$  is the Debye temperature determined from  $C_p^R$ . The magnetic heat capacity is then obtained as  $C_p^R \times \Theta_D^R/\Theta_D^{\text{La}} - C_p^{\text{La}}$  [48]. In the PrCo<sub>2</sub>Al<sub>8</sub> case,  $\Theta_D^{\text{Pr}}$  and  $\Theta_D^{\text{La}}$  were estimated from two methods: assuming the validity of the  $T^3$  Debye law at low- $T$  and by fitting a Debye function plus an optical contribution in some selected  $T$ -intervals (to test the fitting stability) between 15 K and 75 K. The renormalization factors thus obtained ranged from 1.04(2) and 1.006(4). In view of the results, we adopted  $C_p^{\text{La}}$  as a suitable phonon reference in this case (i.e. the renormalization factor is assumed as  $\approx 1$ ).

The Pr magnetic heat capacity was then integrated to find the entropy recovered up to  $T = 25$  K, as shown in figure 5(b). The value at  $\approx 5$  K is already close to  $R \times \ln(2)$ . This result, together with the  $M$  vs.  $H$  curves (Fig. 4(d)), suggests the ordering of a CF pseudo-doublet, associated with all the degrees of freedom in the sample.

In figure 5(c), we present the Pr-based material resistance as function of temperature,  $R(T)$ . The data are normalized by the value of  $R(T)$  measured at  $T = 300$  K. The measurements were performed with the current along the  $c$ -axis. A  $RRR \approx 5$  is found. The first AFM phase transition is clearly observed as a maximum of  $R(T)$  at about  $T \approx 4.9$  K. The inset shows the data derivative and position of the dip in the derivative is very close to  $T_{N1}$  as determined from  $C_p$ . In Fig. 5(d), we compare  $C_p^{\text{Pr}}$  (left axis) with  $d(T\chi_c)/dT$  to pinpoint the values of  $T_{N1}$  and  $T_{N2}$ . The results obtained from the peaks in resistivity, heat capacity and  $d(T\chi_c)/dT$  are in close agreement Fisher [49]. A phase diagram, determined from magnetization measurements (with  $H \parallel c$ ), is presented in figure 5(e).

Experiments of NdCo<sub>2</sub>Al<sub>8</sub> were motivated by the magnetic quantum critical behavior claimed to have been observed in isostructural NdFe<sub>2</sub>Ga<sub>8</sub>, which seems to present the expected behavior of a three dimensional spin density wave type of quantum critical point (QCP) [21, 22]. Our findings show that the NdCo<sub>2</sub>Al<sub>8</sub> case is simpler and similar to that of the Pr-based material. Results are presented in figures 6(a)-(d) and 7(a)-(e). The NdCo<sub>2</sub>Al<sub>8</sub>  $\chi_c$  and  $\chi_{ab}$  data are in figure 6(a) and show that the material is also a strong easy-axis magnet which presents an AFM transition at  $T_N = 8.1$  K. In the inset, we present the analysis of  $\chi_c$  and  $\chi_{ab}$ , obtaining  $\theta_c = 5(3)$  K and  $\theta_{ab} = -125(7)$  K.

To estimate the effective moments and size of the interactions, we examine in figure 6(b)  $\chi_{\text{ave}}$  (left axis) and the inverse of  $(\chi_{\text{ave}} - \chi_0)^{-1}$  (right axis). Here,  $\chi_0 = 2 \times 10^{-4}$  emu/mol.Oe representing the LaCo<sub>2</sub>Al<sub>8</sub> Pauli-like susceptibility. A CW constant ( $\theta_{\text{CW}}^{\text{Nd}}$ ) of  $-43(2)$  K is obtained and suggests AFM interactions. A frustration parameter  $f \approx 5$  is deduced, half of what was obtained for the Pr-based material. The obtained effective moment is  $\mu_{\text{eff}}^{\text{Nd}} = 3.95(5) \mu_B$  which compares well with the theoret-



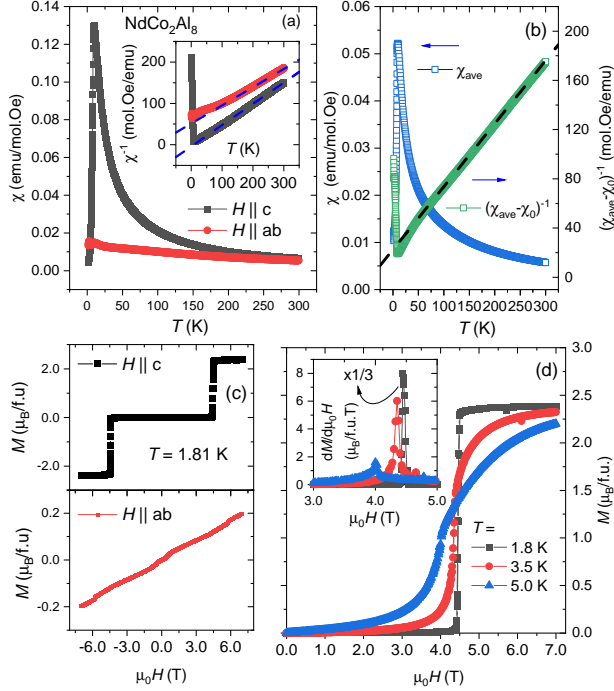


Figure 6.  $\text{NdCo}_2\text{Al}_8$  magnetic properties. (a)  $\chi_c$  and  $\chi_{ab}$  data obtained for  $\mu_0 H = 0.1$  T. From  $\chi_c$ , we deduce an AFM transition at  $T_N = 8.1$  K. In the inset, we present the inverse of  $\chi_a$  and  $\chi_{ab}$  subtracted by  $\chi_0$ . The dashed blue lines represent the CW fitting (obtained for  $T > 100$  K) of the data. (b) Respectively on the left and right axis,  $\chi_{ave}$  and  $(\chi_{ave} - \chi_0)^{-1}$  are presented. The dashed black blue represent the CW fitting of the data (obtained for  $T > 150$  K) (c) Isothermal magnetization curves ( $T = 1.81$  K) obtained with  $H \parallel c$  (upper panel) and  $H \parallel ab$  (lower panel). (d) Representative isothermal magnetization curves for distinct temperatures obtained for  $H \parallel c$ . The data show clear spin-flops transitions from a low field AFM state to a high field polarized metamagnetic state. The inset shows the  $dM/d\mu_0 H$  derivatives from which we determined the critical field for the field-induced metamagnetic transition.

ical value for the  $\text{Nd}^{3+}$  cation ( $3.61 \mu_B$ ). As in the Pr case, the  $\mu_{\text{eff}}^{\text{Nd}}$  value may indicate some contribution from Co, but this is at the edge of our resolution, given the lack of a true polycrystalline average, as discussed above.

Isothermal magnetization measurements at  $T = 1.81$  K, for  $H \parallel c$  (upper panel) and  $H \parallel ab$  (lower panel), are presented in figure 6(c). A metamagnetic transition from a low field AFM state to a high field spin-polarized PM state is observed at about  $\approx 4.5$  T for  $H \parallel c$ . The value of the saturated magnetization corresponds closely to  $2.4 \mu_B/\text{f.u.}$ , which could suggest a  $\alpha \parallel \pm 5/2 \pm \beta \parallel \mp 7/2$  doublet CF ground state with a large  $\parallel \mp 7/2$  component; on the other hand, a higher applied field could lead to another metamagnetic transition with a subsequent  $\mu_{\text{sat}} \approx 3.3 \mu_B$ . In the lower panel, it is shown that relative small fields can generate a spin rotation transition. By comparing the values of the magnetization at 1.81 K

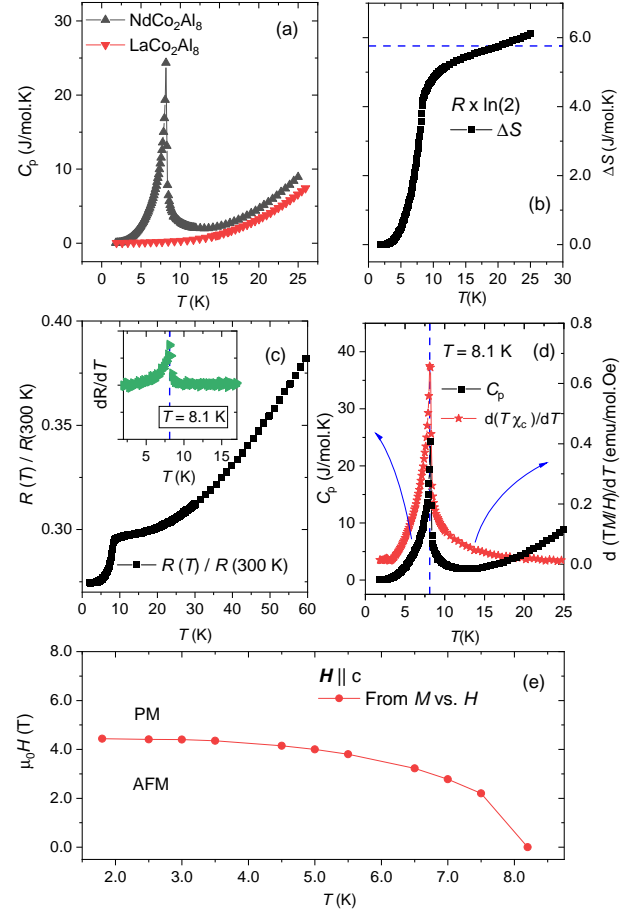


Figure 7.  $\text{NdCo}_2\text{Al}_8$  specific heat and resistance data. (a)  $\text{NdCo}_2\text{Al}_8$   $C_p$  (black triangles) showing the AFM transitions. The  $\text{LaCo}_2\text{Al}_8$   $C_p$  is presented as reference. (b)  $\text{NdCo}_2\text{Al}_8$  magnetic entropy variation (see main text). (c) Temperature dependence of the normalized resistance  $R(T)/R(300 \text{ K})$ . The inset shows the resistance derivative,  $dR/dT$  (d) Comparison between  $C_p$  and  $d(T\chi_c)/dT$  showing  $T_N$  as determined from independent measurements. (e)  $\text{NdCo}_2\text{Al}_8$  magnetic phase diagram deduced from  $M(H)$  ( $H \parallel c$ ) measurements.

and  $\mu_0 H = 7$  T for the two field directions, the magnetic anisotropy in  $\text{NdCo}_2\text{Al}_8$  is about  $\approx 12$ .

In figure 6(d), a series of representative isothermal magnetizations ( $H \parallel c$ ) are presented to examine the temperature dependence of the metamagnetic transition. The field derivative of the magnetization ( $dM/d\mu_0 H$ ) are presented in the inset of the figure. Again, we adopt the field at which the derivatives peak as the critical field for the metamagnetic transition.

The  $\text{LaCo}_2\text{Al}_8$  (reference data) and the  $\text{NdCo}_2\text{Al}_8$   $C_p$  ( $C_p^{\text{Nd}}$ ) are presented in figure 7(a). The latter clearly shows the AFM transition at  $T_N = 8.1$  K. As in the  $\text{PrCo}_2\text{Al}_8$  case, we adopt the  $\text{LaCo}_2\text{Al}_8$   $C_p$  as a reference to estimate the  $\text{NdCo}_2\text{Al}_8$  magnetic heat capacity along with the calculation of a renormalization factor  $\Theta_D^{\text{Nd}}/\Theta_D^{\text{La}}$ . As previously, we also investigated the nor-

malization adopting different methods and temperature ranges for the fittings. The obtained factors lied in between 0.95(4) and 0.91(2). We normalized  $C_p^{\text{Nd}}$  by 0.93 (the average) to obtain the magnetic heat capacity and then the total magnetic entropy recovered for  $T$  up to 25 K. This is shown in figure 6(b) and the result corresponds well to the ordering of a CF doublet ground state associated with all the degrees of freedom in the sample. Indeed, being  $\text{Nd}^{3+}$  a Kramer's cation, the CF scheme in its low symmetry environment should feature five doublets.

The  $\text{NdCo}_2\text{Al}_8$  normalized resistance is shown in figure 7(c). A sharp drop of  $R(T)$  at about 8 K axis marks the AFM transition. The  $RRR$  is also close to  $\approx 5$  as for the other  $R$ -based materials. In the inset, we show the derivative of the normalized resistance and a peak is observed at  $T = 8.1$  K, marking the AFM transition. In 7(d),  $C_p^{\text{Nd}}$  (left axis) and  $d(T\chi_c)/dT$  are compared to pinpoint the value of  $T_N$ , which is confirmed as 8.1 K. We summarize our findings in the phase diagram in figure 7(e).

#### D. $\text{SmCo}_2\text{Al}_8$

The  $\text{SmCo}_2\text{Al}_8$  properties are presented in figures 8(a)-(g). In figure 8(a)  $\chi_c$  and  $\chi_{ab}$  data characterize  $\text{SmCo}_2\text{Al}_8$  as an easy-axis magnet with  $T_N \approx 21.6$  K. In 8(b), we present  $\chi_{\text{ave}}$ . The overall paramagnetic response is small and CW behavior is not observed. This is common for Sm-based intermetallic compounds where the first excited Hund's rule multiplet is low enough so as to contaminate the ground-state multiplet response.

$\text{SmCo}_2\text{Al}_8$  was previously reported as a Pauli paramagnet, wherein Sm cations assume a non-magnetic 2+ valence [32]. A careful inspection of the data is thus required. We first investigate the low- $T$  upturn of the data. We present in figure 6(c) isothermal magnetization measurements measured at  $T = 1.81$  K, with  $H \parallel c$  and  $H \parallel ab$ . The response is small for both field directions and describe the finite response of the AFM state to an applied field. No ferromagnetic component is observed and a paramagnetic component (from any impurity phase) would have a larger response.

The  $\text{LaCo}_2\text{Al}_8$  and  $\text{SmCo}_2\text{Al}_8$   $C_p$  are presented in figure 8(d). The phase transition suggested in figure 8(a) is clearly present in the  $C_p^{\text{Sm}}$  measurements. To normalize the phonon contribution, we modeled  $C_p^{\text{La}}$  and  $C_p^{\text{Sm}}$  in the  $T$ -interval  $28 < T < 75$ , which is well above the transition temperature, taking into account Debye and optical phonons. Indeed, this  $T$ -range lies outside the validity of the  $T^3$  law. The obtained renormalization factor is 0.86(3). We then obtain the  $\text{SmCo}_2\text{Al}_8$  magnetic heat capacity. It is observed that at low- $T$  it becomes slightly negative, certainly because of the uncertainties related with the phonon subtraction. We then integrate it in the interval  $3.3 < T < 30$  K, where it is strictly positive, to find the total recovered magnetic entropy

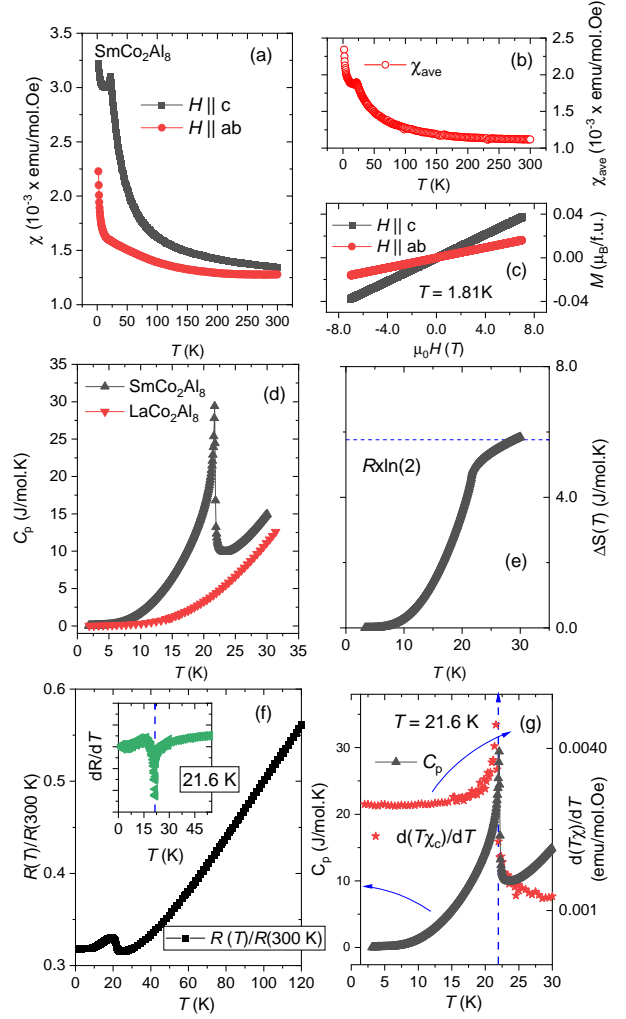


Figure 8.  $\text{SmCo}_2\text{Al}_8$  magnetic, thermal and transport properties. (a)  $\chi_c$  and  $\chi_{ab}$  data obtained for  $\mu_0 H = 0.1$  T. An AFM transition is suggested at  $T_N = 21.6$  K for measurements along the  $c$ -axis. (b)  $\chi_{\text{ave}}$  is presented. CW behavior is not observed in the investigated  $T$ -interval (c) Isothermal magnetization curves ( $T = 1.81$  K) obtained with  $H \parallel c$  and  $H \parallel ab$  (d)  $\text{SmCo}_2\text{Al}_8$   $C_p$  (black triangles) showing the AFM transition at  $T_N = 21.6$  K as suggested by  $\chi$  measurements. The  $\text{LaCo}_2\text{Al}_8$   $C_p$  (red triangles) is presented as reference. (e)  $\text{SmCo}_2\text{Al}_8$  magnetic entropy variation (see main text). (f) Temperature dependence of the normalized resistance  $R(T)/R(300 \text{ K})$ . The inset shows the resistance derivative,  $dR/dT$ . (g) Comparison between  $C_p$  and  $d(T\chi_c)/dT$  determining  $T_N$  from independent measurements.

up to 30 K. Results are shown in figure 8(e). As can be observed,  $R \times \ln(2)$  is obtained at about  $T \approx 29$  K. This result is certainly underestimating the magnetic entropy but, nevertheless, shows that the transition here observed corresponds to the ordering of a well localized ground state CF doublet and suggests the absence of Sm mixed-valence. Moreover, the results give further confidence that the  $\text{SmCo}_2\text{Al}_8$  magnetic response stems from

the whole of the sample and not from an impurity.

The  $\text{SmCo}_2\text{Al}_8$  transport properties are examined in 8(f), where the normalized resistance as a function of  $T$  is presented. The obtained  $RRR$  is close to  $\approx 4$ . A broad peak in  $R(T)$  is observed about  $T \approx 21$  K and can be ascribed to the AFM transition. In the inset, we present the resistance derivative and the peak position in the derivative is identified at  $T = 21.6$  K. Furthermore, results for  $R(T)$  do not support Sm mixed-valence. For a more precise determination of  $T_N$ , we show in Fig. 8(f)  $C_p^{\text{Nd}}$  (left axis) and  $d(T\chi_c)/dT$  (right axis). The AFM transition temperature  $T_N = 21.6$  K is confirmed.

#### IV. SUMMARY AND CONCLUSIONS

We investigated the anisotropic magnetic and transport properties and thermal properties of  $R\text{Co}_2\text{Al}_8$  single crystals ( $R = \text{La, Ce, Pr, Nd, and Sm}$ ).  $\text{LaCo}_2\text{Al}_8$  is a Pauli paramagnet with a resolvable anisotropy in the temperature dependent resistivity.  $\text{CeCo}_2\text{Al}_8$  is a Kondo lattice compound that presents no magnetic order down to 1.81 K. Anisotropic Kondo coherence temperatures  $T_{K,c}^* \approx 68$  K and  $T_{K,ab}^* = 46$  K were estimated from the broad peaks of the Ce 4f contribution to  $\rho_c$  and  $\rho_{ab}$ , respectively. A thermodynamic Kondo temperature was estimated from  $C_p$  and amounts to  $T_K = 36 - 70$  K, depending on the method that is adopted to estimate it.

Based upon these results, we concluded that an anisotropic Kondo state is formed in  $\text{CeCo}_2\text{Al}_8$  in a way that coherent Kondo scattering first sets in along the  $c$ -

axis and then along the  $ab$  plane. This anisotropy likely stems from the conduction electrons anisotropy, measured for both the  $\text{LaCo}_2\text{Al}_8$  and  $\text{CeCo}_2\text{Al}_8$  compounds. In a sense, in the temperature interval in between  $T_{K,c}^*$  and  $T_{K,ab}^*$ , one finds a situation that is similar to what is observed in  $\text{CeCo}_2\text{Ga}_8$  below 17 K, and was termed an axial Kondo chain.

The  $\text{PrCo}_2\text{Al}_8$  and  $\text{NdCo}_2\text{Al}_8$  materials are easy axis AFM materials for which the moments are aligned along the  $c$ -axis. For  $\text{PrCo}_2\text{Al}_8$ , two AFM transitions are observed at zero applied field. The transitions merge into a single transition at low- $T$ . It is safe to assert that in  $\text{PrCo}_2\text{Al}_8$ , the CF ground state is a  $||4\rangle$  singlet making  $\text{PrCo}_2\text{Al}_8$  an Ising-like system.

The  $\text{SmCo}_2\text{Al}_8$  material is an AFM material, but no information about the single ion physics could be extracted, since a CW behavior was not observed. For all AFM materials,  $T_N$  was confirmed by heat capacity, magnetization and resistivity measurements.

#### V. ACKNOWLEDGMENTS

This work was supported by the U.S. Department of Energy, Office of Science, Basic Energy Sciences, Materials Science and Engineering. Ames National Laboratory is operated for the USDOE by Iowa State University under Contract No. DE-AC02-07CH11358. F.G. and C.A. acknowledge, respectively, financial support from the University of Sao Paulo and UNICAMP (sabbatical leave). Ryan Mackenzie is acknowledged for fruitful discussions during the draft of the manuscript.

- 
- [1] A. C. Hewson, *The Kondo Problem to Heavy Fermions*, Cambridge Studies in Magnetism (Cambridge University Press, Cambridge, 1993).
  - [2] P. Coleman and A. J. Schofield, Quantum criticality, *Nature* **433**, 226 (2005).
  - [3] F. Steglich and S. Wirth, Foundations of Heavy-Fermion Superconductivity: Lattice Kondo Effect and Mott Physics, *Reports on Progress in Physics* **79**, 084502 (2016).
  - [4] Y.-F. Yang, An emerging global picture of heavy fermion physics, *Journal of Physics: Condensed Matter Journal of Physics: Condensed Matter* **35**, 103002 (2022).
  - [5] P. Coleman, *Introduction to Many-Body Physics* (Cambridge University Press, 2016).
  - [6] S. L. Bud'ko, Z. Islam, T. A. Wiener, I. R. Fisher, A. H. Lacerda, and P. C. Canfield, Anisotropy and metamagnetism in the  $\text{RNi}_2\text{Ge}_2$  ( $R = \text{Y, La-Nd, Sm-Lu}$ ) series, *Journal of Magnetism and Magnetic Materials* **205**, 53 (1999).
  - [7] A. K. Bhatnagar, K. D. D. Rathnayaka, D. G. Naugle, and P. C. Canfield, Electrical resistivity and thermopower of single-crystal  $\text{RNi}_2\text{Ge}_2$  ( $R=\text{Dy, Ho, Er, Tm}$ ) magnetic superconductors, *Physical Review B* **56**, 437 (1997).
  - [8] P. C. Canfield, S. L. Budko, B. K. Cho, W. P. Beyermann, and A. Yatskar,  $\text{RNi}_2\text{B}_2\text{C}$  magnetic superconductors: An update from the front, *Journal of Alloys and Compounds* **250**, 596 (1997).
  - [9] I. R. Fisher, J. R. Cooper, and P. C. Canfield, Anisotropic resistivity and normal-state magnetoresistance of  $\text{RNi}_2\text{B}_2\text{C}$  ( $R = \text{Y, Lu, Er, Ho}$ ), *Physical Review B* **56**, 10820 (1997).
  - [10] C. Petrovic, S. L. Bud'ko, J. D. Strand, and P. C. Canfield, Anisotropic properties of rare earth silver dibismides, *Journal of Magnetism and Magnetic Materials* **261**, 210 (2003).
  - [11] K. D. Myers, S. L. Bud'ko, I. R. Fisher, Z. Islam, H. Kleinke, A. H. Lacerda, and P. C. Canfield, Systematic study of anisotropic transport and magnetic properties of  $\text{RAgSb}_2$  ( $R = \text{Y, La-Nd, Sm, Gd-Tm}$ ), *Journal of Magnetism and Magnetic Materials* **205**, 27 (1999).
  - [12] P. Canfield, J. Thompson, W. Beyermann, A. Lacerda, M. Hundley, E. Peterson, Z. Fisk, and H. Ott, Magnetism and Heavy Fermion-Like Behavior in the  $\text{RBiPt}$  Series, *Journal of Applied Physics* **70**, 5800 (1991).
  - [13] E. Mun and S. L. Bud'ko,  $\text{RPtBi}$ : Magnetism and topology, *MRS Bulletin* **47**, 609 (2022).

- [14] M. S. Torikachvili, S. Jia, E. D. Mun, S. T. Hannahs, R. C. Black, W. K. Neils, D. Martien, S. L. Bud'ko, and P. C. Canfield, Six closely related  $\text{YbT}_2\text{Zn}_{20}$  ( $T = \text{Fe, Co, Ru, Rh, Os, Ir}$ ) heavy fermion compounds with large local moment degeneracy, *Proceedings of the National Academy of Sciences* **104**, 9960 (2007).
- [15] E. C. Andrade, M. Brando, C. Geibel, and M. Vojta, Competing orders, competing anisotropies, and multicriticality: The case of Co-doped  $\text{YbRh}_2\text{Si}_2$ , *Physical Review B* **90**, 075138 (2014).
- [16] D. Hafner, B. K. Rai, J. Banda, K. Kliemt, C. Krellner, J. Sichelschmidt, E. Morosan, C. Geibel, and M. Brando, Kondo-lattice ferromagnets and their peculiar order along the magnetically hard axis determined by the crystalline electric field, *Physical Review B* **99**, 201109 (2019).
- [17] M. P. Kwasigroch, H. Hu, F. Krüger, and A. G. Green, Magnetic hard-direction ordering in anisotropic Kondo systems, *Physical Review B* **105**, 224418 (2022).
- [18] M. Kornjača and R. Flint, *Distinct effect of Kondo physics on crystal field splitting in electron and spin spectroscopies* (2024), arXiv:2407.09971 [cond-mat].
- [19] W. Xia, W.-S. Tee, P. C. Canfield, F. A. Garcia, R. A. Ribeiro, Y. Lee, L. Ke, R. Flint, and C.-Z. Wang, Machine learning accelerated prediction of Ce-based ternary compounds involving antagonistic pairs, *Physical Review Materials* **9**, 053803 (2025).
- [20] Y. Lee, Z. Ning, R. Flint, R. J. McQueeney, I. I. Mazin, and L. Ke, Importance of enforcing Hund's rules in density functional theory calculations of rare earth magnetocrystalline anisotropy, *npj Computational Materials* **11**, 1 (2025).
- [21] X. Wang, C. Wang, B. Liu, K. Jia, X. Ma, G. Li, X. Wang, C.-W. Wang, Y. Shi, Y.-f. Yang, and S. Li, Neutron diffraction and linear Gruneisen parameter studies of magnetism in  $\text{NdFe}_2\text{Ga}_8$ , *Physical Review B* **105**, 035152 (2022).
- [22] C. Wang, X. Wang, L. Wang, M. Yang, Y. Song, Z. Mi, G. Li, Y. Shi, S. Li, and Y.-f. Yang, Quantum criticality in  $\text{NdFe}_2\text{Ga}_8$  under magnetic field, *Physical Review B* **103**, 035107 (2021).
- [23] S. Zou, H. Zeng, Z. Wang, G. Dong, X. Guo, F. Lu, Z. Zhu, Y. Shi, and Y. Luo, *Abnormal planar Hall effect in quasi-1D Kondo chain  $\text{CeCo}_8\text{Ga}_8$  and its implications for hybridization dynamics* (2024), arXiv:2407.09908 [cond-mat].
- [24] P. Zheng, C. Wang, Y. Xu, L. Wang, W. Wu, Y. G. Shi, Y.-f. Yang, and J. L. Luo, Uniaxial hybridization in the quasi-one-dimensional Kondo lattice  $\text{CeCo}_2\text{Ga}_8$ , *Physical Review B* **105**, 035112 (2022).
- [25] K. Cheng, L. Wang, Y. Xu, F. Yang, H. Zhu, J. Ke, X. Lu, Z. Xia, J. Wang, Y. Shi, Y. Yang, and Y. Luo, Realization of Kondo chain in  $\text{CeCo}_2\text{Ga}_8$ , *Physical Review Materials* **3**, 021402 (2019).
- [26] L. Wang, Z. Fu, J. Sun, M. Liu, W. Yi, C. Yi, Y. Luo, Y. Dai, G. Liu, Y. Matsushita, K. Yamaura, L. Lu, J.-G. Cheng, Y.-f. Yang, Y. Shi, and J. Luo, Heavy fermion behavior in the quasi-one-dimensional Kondo lattice  $\text{CeCo}_2\text{Ga}_8$ , *npj Quantum Materials* **2**, 1 (2017).
- [27] C. Wang, X. Wang, K. Jia, L. Wang, D. Yan, H. L. Feng, S. Li, and Y. Shi, Single-crystal growth and magnetic anisotropy in  $\text{PrFe}_2\text{Ga}_8$ , *Journal of Physics-Condensed Matter* **34**, 165601 (2022).
- [28] J.-J. Xiao, C.-X. Wang, D.-Y. Yan, Y. Li, H. L. Feng, L.-J. Liu, and Y.-G. Shi, Strong magnetic anisotropy in  $\text{PrRu}_2\text{Ga}_8$  and  $\text{PrCo}_2\text{Al}_8$  single crystals, *Journal of Physics-Condensed Matter* **35**, 295601 (2023).
- [29] S. Ghosh and A. M. Strydom, Strongly Correlated Electron Behaviour in  $\text{CeT}_2\text{Al}_8$  ( $T = \text{Fe, Co}$ ), *Acta Physica Polonica A* **121**, 1082 (2012).
- [30] H. S. Nair, S. K. Ghosh, K. R. Kumar, and A. M. Strydom, Magnetic ordering and crystal field effects in quasi-caged structure compound  $\text{PrFe}_2\text{Al}_8$ , *Journal of Physics and Chemistry of Solids* **91**, 69 (2016).
- [31] H. S. Nair, M. O. Ogunbunmi, C. M. N. Kumar, D. T. Adroja, P. Manuel, D. Fortes, J. Taylor, and A. M. Strydom, Pr-magnetism in the quasi-skutterudite compound  $\text{PrFe}_2\text{Al}_8$ , *Journal of Physics-Condensed Matter* **29**, 345801 (2017).
- [32] P. Watkins-Curry, J. V. Burnett, T. Samanta, D. P. Young, S. Stadler, and J. Y. Chan, Strategic Crystal Growth and Physical Properties of Single-Crystalline  $\text{LnCo}_2\text{Al}_8$  ( $\text{Ln} = \text{La-Nd, Sm, Yb}$ ), *Crystal Growth & Design* **15**, 3293 (2015).
- [33] L. J. Treadwell, P. Watkins-Curry, J. D. McAlpin, D. J. Rebar, J. K. Hebert, J. F. DiTusa, and J. Y. Chan, Investigation of Mn, Fe, and Ni Incorporation in  $\text{CeCo}_2\text{Al}_8$ , *Inorganic Chemistry* **54**, 963 (2015).
- [34] P. C. Canfield, New materials physics, *Reports On Progress In Physics* **83**, 016501 (2020).
- [35] *Canfield Crucible Sets | LSP Industrial Ceramics, Inc.*
- [36] O. Moze, L. D. Tung, J. J. M. Franse, and K. H. J. Buschow, Crystal structure and the magnetic properties of the compound  $\text{CeCoAl}_4$ , *Journal of Alloys and Compounds* **256**, 45 (1997).
- [37] L. D. Tung, D. M. Paul, M. R. Lees, P. Schobinger-Papamantellos, and K. H. J. Buschow, Specific heat studies of  $\text{PrCoAl}_4$  single crystal, *Journal of Magnetism and Magnetic Materials* **281**, 378 (2004).
- [38] O. Tougaard and H. Noël, Crystal structures and magnetic properties of  $\text{NdCoAl}_4$ ,  $\text{Nd}_2\text{Co}_3\text{Al}_9$  and  $\text{Sm}_2\text{Co}_3\text{Al}_9$ , *Journal of Alloys and Compounds* **417**, 1 (2006).
- [39] B. H. Toby and R. B. Von Dreele, GSAS-II: the genesis of a modern open-source all purpose crystallography software package, *Journal of Applied Crystallography* **46**, 544 (2013).
- [40] R. P. Hermann, F. Grandjean, and G. J. Long, Einstein oscillators that impede thermal transport, *American Journal of Physics* **73**, 110 (2005).
- [41] H.-J. Tian, P. Qian, J. Shen, and N.-X. Chen, Atomistic simulation on the structure and lattice vibration of  $\text{RCO}_2\text{Al}_8$  ( $R = \text{La, Ce and Pr}$ ), *Computational Materials Science* **44**, 702 (2008).
- [42] G. J. Snyder and E. S. Toberer, Complex thermoelectric materials, *Nature Materials* **7**, 105 (2008).
- [43] J. Mao, Z. Liu, J. Zhou, H. Zhu, Q. Zhang, G. Chen, and Z. Ren, Advances in thermoelectrics, *Advances in Physics* **67**, 69 (2018).
- [44] F. A. Garcia, D. J. Garcia, M. A. Avila, J. M. Vargas, P. G. Pagliuso, C. Rettori, M. C. G. Passeggi, S. B. Os-eroff, P. Schlottmann, B. Alascio, and Z. Fisk, Coexisting on-center and off-center  $\text{Yb}^{3+}$  sites in  $\text{Ce}_{1-x}\text{Yb}_x\text{Fe}_4\text{P}_{12}$  skutterudites, *Physical Review B* **80**, 052401 (2009).
- [45] N. W. Ashcroft and N. D. Mermin, *Solid State Physics* (Holt, Rinehart and Winston, New York, 1976).
- [46] A. Schenck, F. N. Gyax, P. Schobinger-Papamantellos, and L. D. Tung, Multiple magnetic phase transitions in



- PrCoAl<sub>4</sub> observed by muon spin rotation and relaxation measurements, [Physical Review B](#) **71**, 214411 (2005).
- [47] P. Schobinger-Papamantellos, G. André, J. Rodriguez-Carvajal, O. Moze, W. Kockelmann, L. D. Tung, and K. H. J. Buschow, Magnetic ordering of PrCoAl<sub>4</sub> a neutron diffraction study, [Journal of Magnetism and Magnetic Materials](#) **231**, 162 (2001).
- [48] M. Bouvier, P. Lethuillier, and D. Schmitt, Specific heat in some gadolinium compounds. I. Experimental, [Physical Review B](#) **43**, 13137 (1991).
- [49] M. E. Fisher, Relation between the specific heat and susceptibility of an antiferromagnet, [The Philosophical Magazine: A Journal of Theoretical Experimental and Applied Physics](#) **7**, 1731 (1962).